Nonlinear scattering in nanoscale magnetic elements: Overpopulation of the lowest-frequency magnon state

Vladislav E. Demidov, Henning Ulrichs, Sergej O. Demokritov, and Sergei Urazhdin

Phys. Rev. B **83**, 020404 — Published 11 January 2011

DOI: 10.1103/PhysRevB.83.020404

Overpopulation of the lowest-frequency magnon state in nanoscale magnetic elements

Vladislav E. Demidov, Henning Ulrichs, and Sergej O. Demokritov

Institute for Applied Physics and Center for Nonlinear Science, University of Muenster, Corrensstasse 2-4, 48149 Muenster, Germany

Sergei Urazhdin

Department of Physics, West Virginia University, Morgantown, WV 26506, USA

We utilized Brillouin light scattering spectroscopy to study the magnetization dynamics in nanoscale Permalloy elements driven by a large microwave magnetic field. We demonstrate that at large precession angles, the magnons excited by the microwaves scatter into the lowest-frequency state by a process similar to the scattering that leads to the Bose-Einstein condensation of magnons in the low-loss garnet films. The discovered effect is important for understanding the nonlinear processes in strongly driven nanomagnetic devices such as spin-torque nano-oscillators and magnetic memory.

PACS numbers: 75.40.Gb, 85.75.-d, 75.30.Ds, 75.75.-c

* Corresponding author, e-mail: demidov@uni-muenster.de

The subject of strongly nonlinear magnetization dynamics in magnetic nanostructures has recently received significant attention in connection with the discovery and subsequent extensive studies of spin transfer effects [1-7]. Spin transfer can induce very large amplitudes of magnetization oscillation characterized by precession angles reaching tens of degrees, which is important for the implementation of high-frequency nanoscale signal processing devices for communication and data processing technologies [8-11]. The large-amplitude oscillations are generally associated with strongly nonlinear dynamical processes, leading to significant complexity and diversity of the observed behaviors [12-14]. The possibilities for the experimental studies of these nonlinear processes are usually limited due to the lack of direct access to the nanomagnetic elements buried under the electrical leads. As a consequence, the majority of the studies have relied on measurements of the high-frequency electrical signals produced by the oscillations due to the magnetoresistance effect, with a few exceptions such as x-ray dichroism studies of the magnetization reversal [15,16], and the Brillouin light scattering (BLS) spectroscopy of spin waves emitted outside the active area of spin torque-induced excitation [17].

To overcome the limitations imposed by the spin-torque device geometry on the experimental investigations of nonlinear magnetization dynamics, one can instead utilize excitation by a strong microwave magnetic field [18-21]. This approach allows one to precisely control the driving strength and access the magnetization dynamics in individual nanoelements by magneto-optical techniques. Excitation by a large microwave field was successfully applied for the observation of nonlinear hybridization of eigenmodes in Permalloy microstructures [21]. However, the driving microwave field amplitudes achieved in Ref. 21 were insufficient to obtain magnetization precession

angles comparable to those typical for spin-torque devices, resulting in only moderate nonlinear effects.

Here we report the BLS study of large-amplitude magnetization dynamics in nanoscale magnetic elements strongly driven by high-efficiency excitation elements integrated into the nanostructure. Our samples enabled excitation of precession angles comparable to those in spin-torque devices. In addition to the well-known moderately nonlinear phenomena such as the nonlinear resonance, we were able to observe strongly nonlinear magnon scattering leading to the accumulation of magnons in the lowest-frequency state. This phenomenon was previously observed in low-loss garnet films at relatively small precession angles [22,23], and was shown to result in room-temperature Bose-Einstein condensation (BEC) of magnons [24].

The findings reported here suggest that the mechanisms of strongly nonlinear magnon scattering are universal, since similar behaviors are found in magnetic systems with considerably different nonlinear and relaxation properties. Moreover, our results also indicate that the overpopulation of the lowest-frequency magnon state characteristic of BEC is possible in magnetic metals as well as the insulating garnets. These processes are expected to strongly affect the magnetization dynamics of magnetic systems brought far out of equilibrium, and therefore must be taken into account in the analysis and design of nanomagnetic devices.

Our samples were 10-nm-thick elliptical Permalloy elements patterned by ion etching on top of a 160-nm-thick and 1-μm-wide Au microstrip, as schematically shown in Fig. 1. The microstrip was connected to a matched coplanar microwave transmission line. Three Permalloy elements with lateral dimensions of 1000×500 nm, 500×250 nm, and 250×125 nm were used in our study. The edge-to-edge separation between the

elements was 1 μm, rendering them dynamically and statically uncoupled. The entire structure was covered by a 50-nm thick SiO_2 protection layer. The sample was placed into a uniform static magnetic field H=400-900 Oe applied parallel to the direction of the microstrip. The driving microwave magnetic field h oriented perpendicular to the static field was produced by short pulses of microwave current through the microstrip. The pulses had a 100 ns width and 2 μs repetition period. The low duty cycle of the driving signal minimized the heating effects. The detection of the dynamic magnetization was performed by micro-focus Brillouin light scattering spectroscopy described in detail elsewhere [25]. This technique yields a signal proportional to the square of the amplitude of the dynamic magnetization at the location of the focal spot of the probing light, and provides information about the magnetization dynamics with simultaneous temporal, spectral, and spatial resolution.

The Permalloy nanoelements were characterized by measurements of the dependence of their dynamical response on the driving frequency in the linear regime (at small microwave power), and in the moderately nonlinear regime, as illustrated in Fig. 2 for the element with dimensions of 500×250 nm. Figure 2(a) shows resonant curves for three different values of the excitation power P, measured by varying the excitation frequency f from 8 to 11 GHz and recording the BLS intensity at the same frequency. At small microwave powers, the dependence of the BLS intensity on f exhibits the usual linear resonance line shape, as illustrated for P=0.01 mW in Fig. 2(a). A Lorentizan function [shaded area in Fig. 2(a)] provides a good fit to these data. At larger microwave powers, the resonance becomes increasingly asymmetric due to the sharpening of the rising part of the curve and broadening of its high-frequency tail. This behavior can be explained by the effects of the nonlinear damping and negative

nonlinear frequency shift, as analyzed in detail in Refs. 26-28. We note that the anomalous positive nonlinear frequency shift [21] was not observed in the studied samples due to the low efficiency of the edge mode excitation.

Figure 2(b) summarizes the dependence of the resonant curve linewidth δf measured at one half of the maximum value (squares) and the BLS intensity at the resonant frequency f_r=9.73 GHz (circles) on the microwave power in the range from 0.01 to 1 mW. From the data of Fig. 2(b), one can conclude that the nonlinear effects become significant around $P=P_1\approx0.04$ mW, where the increase of the BLS intensity with P falls significantly below the low-power linear dependence, and the broadening of the resonant curve accelerates. Note that P_1 is about three orders of magnitude smaller than the value obtained in Ref. 21, due to the higher efficiency of the microwave excitation by the smaller microstrip, and more precise impedance matching among the microstrip, the sample leads, and the microwave source.

Figure 3 illustrates the strongly nonlinear dynamics induced at $P>1$ mW, at a fixed excitation frequency $f=f_r$=9.73 GHz. The dependence of the BLS intensity measured at the same frequency initially exhibits a gradual increase with P, similar to the moderately nonlinear low-power behavior [Fig.2(b)]. The increase continues up to P=4 mW, above which the BLS intensity abruptly drops, suggesting an onset of an additional nonlinear effect. To identify this effect, we measured the complete BLS spectra covering the detection frequency range of 4 to 14 GHz, at P between 1 and 100 mW [Fig. 3(b)]. These data clearly demonstrate that, in addition to the usual dynamic magnetization response at the excitation frequency of 9.73 GHz, a second spectral peak appears at 8.12 GHz above the threshold power $P=P_2$. Above the onset, the intensity of this peak initially increases. The decrease of intensity at higher powers is accompanied by the

spectral broadening of the peak. The central frequency f_{sc} of the peak monotonically decreases by 2 GHz as P is increased from P_2 to 100 mW. These findings suggest that the observed phenomenon represents scattering of the excited magnons into a certain magnon state with frequency f_{sc}. The relatively modest variation of f_{sc} with P is likely caused by the nonlinear frequency shift.

To identify the magnon state with frequency f_{sc}, we performed BLS measurements similar to those described by Fig. 3(b) for different values of the static field H. From these measurements we determined the field dependence of the linear-regime (P=0.01 mW) frequency of the resonant mode f_r and the frequency of the secondary mode corresponding to the threshold power $P=P_2$. Figure 4 shows the obtained frequencies (f_r – circles, f_{sc} – squares) and their comparison with the frequencies of the center and the edge modes calculated using OOMMF software [29] for the experimental geometry of the elliptical element and the established room-temperature parameters of Permalloy. The data of Fig. 4 show that the experimental and calculated frequencies of the center mode are in excellent agreement, which proves the validity of the calculations. Meanwhile, the calculated frequency of the edge mode is clearly below the frequency $f_{sc}(P_2)$, and its dependence on the magnetic field exhibits a different slope. Therefore, we concluded that the observed nonlinear scattering is not associated with the edge modes, which was also confirmed by the spatially-resolved measurements, as described below.

Investigations of strongly-nonlinear magnon scattering in low-loss garnet films have shown that, at sufficiently large amplitudes of dynamic magnetization, magnons begin to overpopulate the lowest-frequency state of the magnon spectrum [22,23], under certain conditions resulting in their Bose-Einstein condensation [24]. The location of

this state in the magnon spectrum is shown in a qualitative diagram of the spectrum for an in-plane magnetized ferromagnetic film (inset in Fig. 4) [22]. The solid curves represent the dispersion for the two limiting magnon branches with wave vectors **k** oriented perpendicular and parallel to the static magnetic field **H**, respectively. The latter contains a state with a finite frequency f_0, which is the lowest allowed frequency of magnons. Strictly speaking, the shown spectrum is valid for a continuous magnetic film only, whereas in the case of a nano-element the spectrum is quantized. Nevertheless, as described below, spin waves corresponding to the lowest-frequency state can be excited in a nano-element independently of its geometry, provided the excitation is local and the system is characterized by a non-zero damping.

To determine whether the additional peak observed in our measurements above the threshold P_2 is associated with scattering into the lowest-frequency state, we analytically calculated f_0 using the theory of spin-wave dispersion developed in Ref. 30. In our calculations, we took into account the demagnetization effects due to the finite dimensions of the elliptical elements by using the value of the internal magnetic field obtained from the OOMMF simulations. The calculated dependence $f_0(H)$, shown in Fig. 4 by a dashed curve, is in excellent agreement with the experimentally determined $f_{sc}(P_2)$.

We found further evidence for the overpopulation of the lowest-frequency state by performing two-dimensional imaging of the dynamic magnetization in one of the studied elements with dimensions of 1000×500 nm. Panels (a) and (b) in Fig. 5 show the pseudo-color spatial maps of the intensity of magnetization oscillations at f_{sc}, measured at $P=P_2$ and $P=4P_2$, respectively. The data of Fig. 5 show that, at the onset of the overpopulation, the magnetization oscillations at f_{sc} are well localized near the

center of the element, while at larger P they gradually expand to the entire area of the ellipse.

To analyze this result, we note that the spatial distribution corresponding to the lowest-frequency magnon state must be correlated with the distribution of the resonant state, which is the source of the lowest-frequency magnons. The spatial distribution of the resonant mode is not uniform in space and has a maximum in the center of the ellipse (see the map in Fig. 1). Therefore, the threshold condition for the overpopulation of the lowest-frequency state is first satisfied near the center. Since the magnons at the spectral minimum f_0 are characterized by zero group velocity (see inset in Fig. 4), they do not propagate toward the edges, and the magnetization oscillations at f_0 remain localized. As P increases above P_2, the threshold condition is satisfied over a larger area, leading to the spatial expansion of oscillations at f_0 towards the edges of the ellipse. This spatial expansion can also explain the spectral broadening of the peak at large P shown in Fig. 3(b). The internal magnetic field determined by the superposition of the applied field and the local demagnetizing field of the ellipse is spatially non-uniform. As a consequence, the frequency f_0 also varies in space, resulting in the broadening of the averaged lowest-frequency magnon peak when the oscillations spread over a significant portion of the magnetic element.

Finally, to estimate the relevance of the observed nonlinear behaviors to the large-amplitude oscillations in spin-torque measurements, we calculate the reduction of the projection M_z of the magnetization vector **M** onto the precession axis z, characterizing the magnetization precession angles achieved in our experiments. The estimate can be made based on the observed nonlinear shift of frequency f_{sc} with P [see Fig. 3(b)]. We assume that this shift is determined by the reduction of the projection M_z as a result of

the large-amplitude magnetization precession. Using the theory of Ref. 30, we obtained the dependence of M_z/M on the microwave power. The results of these calculations show that the overpopulation of the lowest-frequency state starts at $M_z/M \approx 0.96$ and the smallest normalized projection achieved in our experiments is about $M_z/M \approx 0.5$. Calculating the mean precession angle φ as $\cos^{-1}(M_z/M)$, the largest value of φ achieved in our measurements is 59° and the angle corresponding to the onset of the overpopulation is about 17°. We emphasize that the angle φ characterizes all the magnetization oscillations over the entire spectrum, and not just the resonant-frequency precession. We also note that the estimated onset angle is much larger compared to that typical for garnet films [22-24], which can be associated with much larger magnetic losses in Permalloy.

In conclusion, we experimentally realized excitation of magnetization dynamics with precession angles of several tens of degrees in nano-sized Permalloy elements driven by a large microwave field. We have observed nonlinear scattering of the excited magnons into the lowest-frequency magnon state and a strong overpopulation of the latter, which was previously found only in the low-loss garnet films. In contrast to the garnet films, the overpopulation in Permalloy structures is accompanied by a strong nonlinear shift of the lowest-frequency state and is strongly influenced by the demagnetization effects. Our findings prove the universal character of this type of magnon dynamics and show that it should be considered in modeling of intense magnetization oscillations. The discovered nonlinear scattering mechanisms should also be taken into account in the design of nanomagnetic devices operating at large precession amplitudes.

We acknowledge support from Deutsche Forschungsgemeinschaft, the European Project Master (No. NMP-FP7 212257), the NSF grants DMR-0747609 and ECCS-0967195, and the Research Corporation.

REFERENCES

[1] E. B. Myers, D. C. Ralph, J. A. Katine, R. N. Louie, and R. A. Buhrman, Science **285**, 867-870 (1999).

[2] J. A. Katine, F. J. Albert, R. A. Buhrman, E. B. Myers, and D. C. Ralph, Phys. Rev. Lett. **84**, 3149-3152 (2000).

[3] M. Tsoi, A. G. M. Jansen, J. Bass, W.-C. Chiang, V. Tsoi, and P. Wyder, Nature **406**, 46-48 (2000).

[4] S. I. Kiselev, J. C. Sankey, I. N. Krivorotov, N. C. Emley, R. J. Schoelkopf, R. A. Buhrman, and D. C. Ralph, Nature **425**, 380-383 (2003).

[5] S. Urazhdin, N. O. Birge, W. P. Pratt, Jr., and J. Bass, Phys. Rev. Lett. **91**, 146803 (2003).

[6] W. H. Rippard, M. R. Pufall, S. Kaka, S. E. Russek, and T. J. Silva, Phys. Rev. Lett. **92**, 27201 (2004).

[7] I. N. Krivorotov, N. C. Emley, J. C. Sankey, S. I. Kiselev, D. C. Ralph, and R. A. Buhrman, Science **307**, 228-231 (2005).

[8] F. B. Mancoff, N. D. Rizzo, B. N. Engel, and S. Tehrani, Nature **437**, 393-395 (2005).

[9] S. Kaka, M. R. Pufall, W. H. Rippard, T. J. Silva, S. E. Russek, and J. A. Katine, Nature **437**, 389-392 (2005).

[10] A. Slavin, Nature Nanotechnology **4**, 479–480 (2009).

[11] A. Ruotolo, V. Cros, B. Georges, A. Dussaux, J. Grollier, C. Deranlot, R. Guillemet, K. Bouzehouane, S. Fusil, and A. Fert, Nature Nanotechnology **4**, 528 - 532 (2009).

[12] A. Slavin and V. Tiberkevich, Phys. Rev. Lett. **95**, 237201 (2005).

[13] J.-V. Kim, Q. Mistral, C. Chappert, V. S. Tiberkevich, and A. N. Slavin, Phys. Rev. Lett. **100**, 167201 (2008).

[14] S. Urazhdin, P. Tabor, V. Tiberkevich, and A. Slavin, Phys. Rev. Lett. **105**, 104101 (2010).

[15] Y. Acremann, J. P. Strachan, V. Chembrolu, S. D. Andrews, T. Tyliszczak, J. A. Katine, M. J. Carey, B. M. Clemens, H. C. Siegmann, and J. Stöhr, Phys. Rev. Lett. **96**, 217202 (2006)

[16] J. P. Strachan, V. Chembrolu, Y. Acremann, X.W. Yu, A. A. Tulapurkar, T. Tyliszczak, J. A. Katine, M. J. Carey, M. R. Scheinfein, H. C. Siegmann, and J. Stöhr, Phys. Rev. Lett. **100**, 247201 (2008).

[17] V. E. Demidov, S. Urazhdin, and S. O. Demokritov, Nature Materials **9**, 984-988 (2010).

[18] J. Podbielski, D. Heitmann, and D. Grundler, Phys. Rev. Lett. **99,** 207202 (2007).

[19] G. Woltersdorf and C. H. Back, Phys. Rev. Lett. **99,** 227207 (2007).

[20] K. S. Buchanan, M. Grimsditch, F.Y. Fradin, S. D. Bader, and V. Novosad, Phys. Rev. Lett. **99,** 267201 (2007).

[21] V. E. Demidov, M. Buchmeier, K. Rott, P. Krzysteczko, J. Münchenberger, G. Reiss, and S. O. Demokritov, Phys. Rev. Lett. **104**, 217203 (2010).

[22] V. E. Demidov, O. Dzyapko, S. O. Demokritov, G. A. Melkov, and A. N. Slavin, Phys. Rev. Lett. **99**, 037205 (2007).

[23] V. E. Demidov, O. Dzyapko, M. Buchmeier, T. Stockhoff, G. Schmitz, G. A. Melkov, and S. O. Demokritov, Phys. Rev. Lett. **101**, 257201 (2008).

[24] S. O. Demokritov, V. E. Demidov, O. Dzyapko, G. A. Melkov, A. A. Serga, B. Hillebrands, and A. N. Slavin, Nature **443**, 430 (2006).

[25] S. O. Demokritov and V.E. Demidov, IEEE Trans. Mag. **44**, 6 (2008).

[26] T. Gerrits, P. Krivosik, M. L. Schneider, C. E. Patton, and T. J. Silva, Phys. Rev. Lett. **98,** 207602 (2007).

[27] Y. S. Gui, A. Wirthmann, and C.-M. Hu, Phys. Rev. B **80**, 184422 (2009).

[28] Y. Khivintsev, B. Kuanr, T. J. Fal, M. Haftel, R. E. Camley, Z. Celinski, and D. L. Mills, Phys. Rev. B **81**, 054436 (2010).

[29] M. Donahue, D.G. Porter, OOMMF User's guide, Version 1.0, Interagency Report NISTIR 6376, NIST, Gaithersburg, MD, 1999, URL: http://math.nist.gov/oommf.

[30] B.A. Kalinikos, IEE Proc. H **127**, 4 (1980).

FIGURE CAPTIONS

FIG. 1. (Color online) Schematic of the experiment. A typical measured map of the intensity of magnetization oscillations corresponding to the resonant center mode is superimposed on the largest elliptical element. Inset shows an SEM micrograph of a section of the microstrip with the 500×250 nm Py nanoelement.

FIG. 2. (Color online) (a) Resonant curves for the ellipse with dimensions of 500×250 nm, at three different values of the applied microwave power P, as labeled. The shaded area is a Lorentzian fit of the P=0.01 mW data. (b) Dependence of the BLS intensity at the resonant frequency f_r=9.73 GHz (circles) and of the resonant curve width δf (squares) on the applied microwave power. Lines are guides to the eye. All measurements were performed at H = 900 Oe.

FIG. 3. (Color online) (a) BLS intensity *vs* microwave power in the strongly nonlinear regime. (b) Logarithmic-scale pseudo-color plot of the BLS intensity as a function of the microwave power and the detection frequency. All data were acquired with the excitation frequency fixed at 9.73 GHz.

FIG. 4. (Color online) Dependence of the dynamical characteristics on the static magnetic field H: circles – low-amplitude linear resonant frequency, squares – frequency of the state into which the magnons are scattered at $P=P_2$, solid curves – calculated frequencies of the center and the edge modes, as labeled, dashed curve – calculated lowest magnon frequency. Inset qualitatively shows the magnon spectrum for a magnetic film magnetized in-plane.

FIG. 5. (Color online) Normalized pseudo-color spatial intensity maps of magnetization oscillations at f_{sc}, measured at $P = P_2$ (a) and $P = 4P_2$ (b). The dimensions of the maps are 1100×600 nm, and the spatial step size is 50 nm.

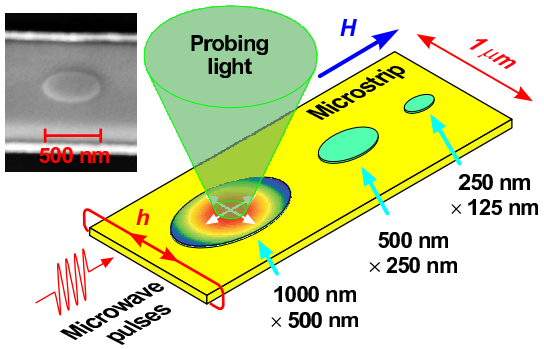

Figure 1 LX11947BR 29NOV2010

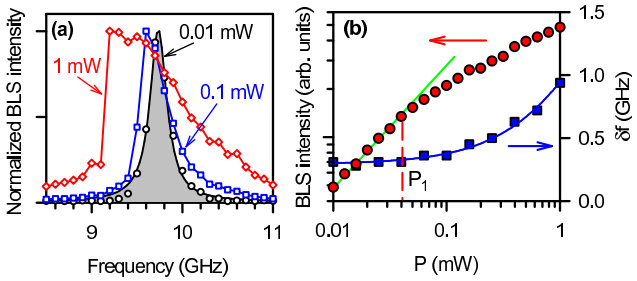

Figure 2 LX11947BR 29NOV2010

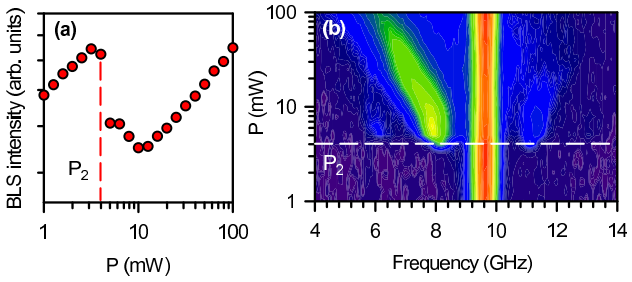

Figure 3 LX11947BR 29NOV2010

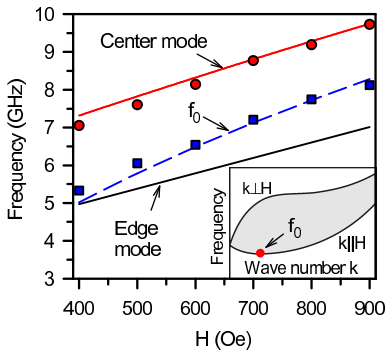

Figure 4 LX11947BR 29NOV2010

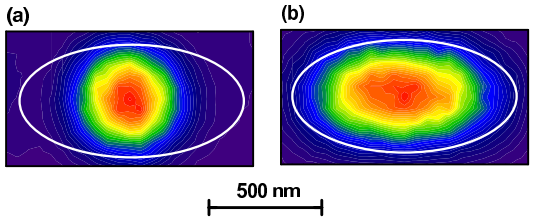

Figure 5 LX11947BR 29NOV2010